

Coherent strong-field control of multiple states by a single chirped femtosecond laser pulse

M Krug, T Bayer, M Wollenhaupt, C Sarpe-Tudoran and T Baumert

Universität Kassel, Institut für Physik und CINSaT, Heinrich-Plett-Str. 40, D-34132 Kassel, Germany

E-mail: wollenha@physik.uni-kassel.de, tbaumert@physik.uni-kassel.de

S S Ivanov¹ and N V Vitanov^{1,2}

¹ Department of Physics, Sofia University, James Bourchier 5 blvd, 1164 Sofia, Bulgaria

² Institute of Solid State Physics, Bulgarian Academy of Sciences, Tsarigradsko chaussée 72, 1784 Sofia, Bulgaria

E-mail: vitanov@phys.uni-sofia.bg

Abstract. We present a joint experimental and theoretical study on strong-field photo-ionization of sodium atoms using chirped femtosecond laser pulses. By tuning the chirp parameter, selectivity among the population in the highly excited states $5p$, $6p$, $7p$ and $5f$, $6f$ is achieved. Different excitation pathways enabling control are identified by simultaneous ionization and measurement of photoelectron angular distributions employing the velocity map imaging technique. Free electron wave packets at an energy of around 1 eV are observed. These photoelectrons originate from two channels. The predominant $2+1+1$ Resonance Enhanced Multi-Photon Ionization (REMPI) proceeds via the strongly driven two-photon transition $4s \leftarrow \leftarrow 3s$, and subsequent ionization from the states $5p$, $6p$ and $7p$ whereas the second pathway involves $3+1$ REMPI via the states $5f$ and $6f$. In addition, electron wave packets from two-photon ionization of the non-resonant transiently populated state $3p$ are observed close to the ionization threshold. A mainly qualitative five-state model for the predominant excitation channel is studied theoretically to provide insights into the physical mechanisms at play. Our analysis shows that by tuning the chirp parameter the dynamics is effectively controlled by dynamic Stark-shifts and level crossings. In particular, we show that under the experimental conditions the passage through an uncommon three-state “bow-tie” level crossing allows the preparation of coherent superposition states.

PACS numbers: 32.80.Qk, 32.80.Rm, 33.80.Rv

1. Introduction

Selective excitation of preselected target states making use of shaped femtosecond laser pulses is at the heart of coherent quantum control [1, 2, 3, 4, 5, 6, 7, 8, 9, 10]. Closed-loop optimization strategies [4, 11, 12, 13, 14, 15] have proven enormously successful in controlling a huge variety of quantum systems, however studies on model systems employing defined pulse shapes are the key to better understand the underlying physical mechanisms and to further develop quantum control concepts and techniques. This applies in particular to *strong-field* quantum control [16, 17, 18, 19, 20] characterized by non-perturbative interaction of a quantum system with intense shaped laser pulses. Strong-field physical mechanisms involve—besides the interference of multiple excitation pathways—adiabatic and non-adiabatic time evolution accompanied by Dynamic Stark-Shifts (DSSs) in the order of hundreds of meV. The latter is responsible for modification of the atomic states or molecular potential surfaces [21, 22, 23] such that new pathways become available and new target states—inaccessible in weak laser fields—open up. Recent studies of strong-field control on model systems devoted to the analysis of the basic physical mechanisms revealed that the concept of Selective Population of Dressed States (SPODS) [24] provides a natural description of controlled dynamics in intense shaped laser fields. For example, it was shown that ultrafast switching among different target channels by phase discontinuities within the pulse [16, 24, 25, 26], Rapid Adiabatic Passage (RAP) by chirped pulses [27] and combinations thereof [28] are realizations of this general concept.

Chirped pulses are a well-established tool in quantum control because they usually serve as a prototype for shaped pulses with controllable envelope and time-varying instantaneous frequency. Therefore, they have played a prominent role in the development of quantum control concepts and techniques and are still the “workhorse” to test novel strategies in quantum control. Examples of quantum control with chirped pulses comprise studies of selective excitation and ionization of multi-level system in alkali atoms [19, 27, 29, 30, 31, 32, 33, 34], control of molecular dynamics in diatomics and dyes [35, 36, 37, 38, 39, 40, 41, 42], measurement of coherent transients [43] and the development of adiabatic passage techniques [44].

In the present contribution we employ chirped ultrashort laser pulses resulting from phase modulation of the laser spectrum to study Resonance Enhanced Multi-Photon Ionization (REMPI) of a multi-level system in sodium atoms. We demonstrate experimentally, that different excitation pathways and, accordingly, different target channels can be addressed selectively by a single control parameter, i.e. the chirp. The nature of these pathways is unraveled by measurement of Photoelectron Angular Distributions (PADs) from Velocity Map Imaging (VMI) [45, 46, 47, 48, 49, 50], yielding detailed information on the origin of the released photoelectron wave packets. Theoretical investigations of the light-atom interaction reveal an interplay of different physical mechanisms governing control. Analysis of the neutral excitation dynamics for a five-state model-atom (including the most relevant states $3s$, $4s$, $5p$, $6p$ and $7p$) under

influence of a chirped ultrashort laser pulse highlights how physical mechanisms, such as RAP and DSS, act jointly to either address single states among the high lying sodium states $5p$, $6p$ and $7p$ (cf. Fig. 1), or excite superpositions of any two neighboring states. We point out that the present paper extends two earlier techniques in several significant directions. The technique of Melinger *et al.* [29] uses a single chirped picosecond laser pulse to selectively excite the two fine-structure components $3p_{1/2}$ and $3p_{3/2}$ in sodium atoms. The present technique adds a DSS to the control tools, which enables the population of a third state, and also the creation of coherent superposition states. The technique of Clow *et al.* [34] makes use of a shaped femtosecond pulse to selectively populate a single highly excited state. The present technique is more flexible, since it allows to populate several different states by variation of a single parameter: the chirp.

The article is organized as follows. We start in Sec. 2 by introducing the excitation and ionization scheme of sodium atoms exposed to ultrashort near-infrared laser pulses, and subsequently describe the details of our experimental setup. The experimental results are presented in Sec. 3 along with a physical discussion of general features observed in the measured PADs supported by numerical simulations of the measurement results. Sec. 4 provides a detailed theoretical analysis of the strong-field induced chirped excitation dynamics in terms of adiabatic states, highlighting different physical mechanisms that govern the light-atom interaction. We conclude the paper with a brief summary and conclusions.

2. Experiment

In our experiment, we combine spectral phase shaping to produce chirped ultrashort laser pulses with the measurement of PADs resulting from REMPI of sodium atoms, employing the VMI technique. In this section, we first introduce the sodium excitation scheme with emphasis on the different accessible excitation and ionization pathways. Then we describe the experimental setup and layout of our photoelectron imaging spectrometer.

2.1. Excitation scheme

Fig. 1 shows the excitation and ionization scheme of sodium atoms based on energy level information taken from the NIST-database [51]. Different multi-photon excitation pathways are accessible during the interaction of sodium atoms with intense ultrashort laser pulses (laser specifications are given in Sec. 2.2). The predominant excitation pathway is a 2+1+1 REMPI process via the two-photon transition $4s \leftarrow \leftarrow 3s$ (red arrows in Fig. 1) which is nearly resonant with our laser spectrum [52]. Consequential population of states $5p$, $6p$ and $7p$ gives rise to photoelectron wave packets in the ionization continuum having s or d -symmetry. The recorded PADs therefore exhibit a combined s and d -symmetry and are measured at the distinct kinetic energies 0.76 eV, 1.04 eV and 1.20 eV, corresponding to states $5p$, $6p$ and $7p$ respectively. Alternatively,

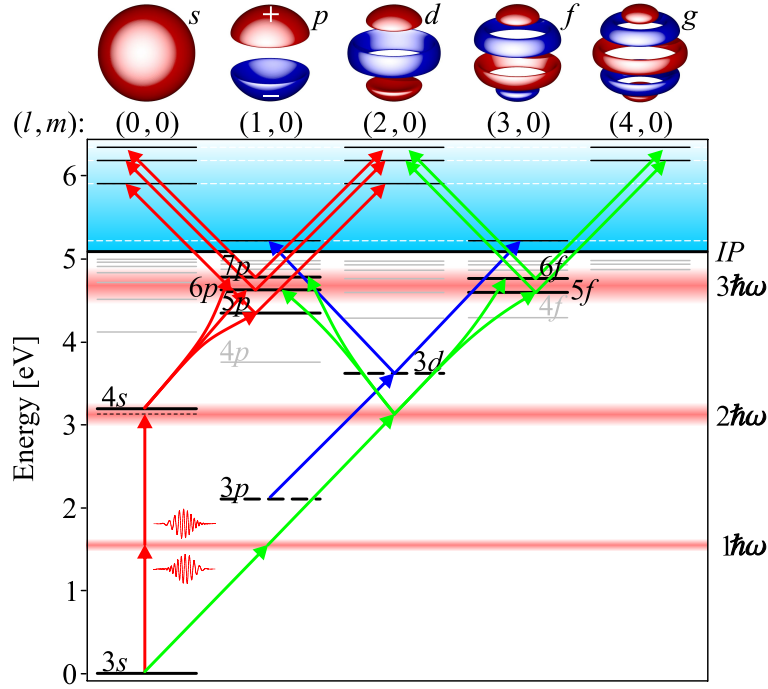


Figure 1. (Color online) excitation and ionization scheme of sodium atoms illustrating the excitation pathways that arise during the interaction with an intense 795 nm, 30 fs FWHM laser pulse. These pathways comprise a 2+1+1 REMPI (red arrows) and a 3+1 REMPI (green arrows) process from the 3s ground state as well as a two-photon ionization process from state 3p (blue arrows). Blurred red bars represent the one, two and three-photon spectrum of our laser respectively. Since state 4s lies within the bandwidth of the two-photon spectrum, the laser strongly drives the transition $4s \leftarrow 3s$. Once state 4s is populated, population flows to states 5p, 6p and 7p, giving rise to photoelectron wave packets with combined s and d-symmetry at characteristic kinetic energies 0.76 eV, 1.04 eV and 1.20 eV in the ionization continuum. A competing excitation pathway is opened up by three-photon absorption leading to population of states 5f and 6f in addition. Photoelectrons from this excitation channel are characterized by a combined d and g-symmetry of the measured PADs at kinetic energies 1.02 eV and 1.18 eV respectively. Two-photon ionization from the non-resonant, transiently populated state 3p results in photoelectron wave packets at about 0.2 eV, having combined p and f-symmetry. For illustrative purposes, the relevant symmetries of the released photoelectron wave packets are visualized on top of the figure in red and blue, encoding the positive and negative sign of the electron wave function respectively.

a 3+1 REMPI process (green arrows in Fig. 1) based on three-photon absorption from the 3s ground state with no intermediate resonances is taken into account, contributing also to the population of states 5p, 6p and 7p but, in addition, transferring population to states 5f and 6f. One-photon ionization of the latter results in photoelectron wave packets with d and g-symmetry at kinetic energies 1.02 eV and 1.18 eV respectively. These photoelectrons are distinguished from the p state contributions (at 1.04 eV and 1.20 eV) by the symmetry of their angular distributions. In the following we will refer to

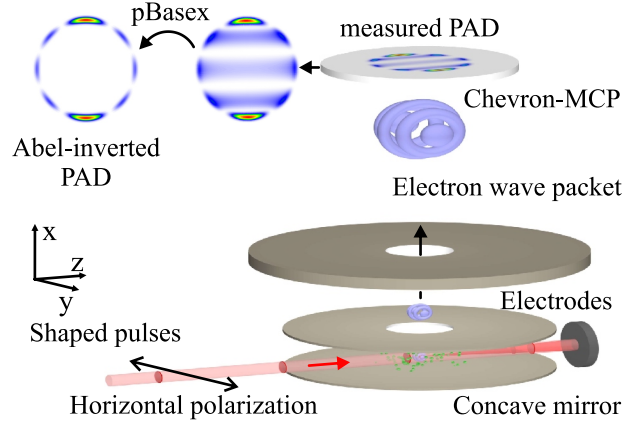


Figure 2. (Color online) experimental setup. Horizontally polarized femtosecond laser pulses are sent into a vacuum chamber and refocused by a 50 mm on-axis concave mirror into sodium vapor provided by an alkali metal dispenser source (not shown). Photoelectrons emitted by the light-atom interaction are projected towards a position sensitive MCP-detector using the VMI method. The amplified signal is recorded by a 1.4 million pixels camera-system and sent to a computer. An Abel-inversion is performed using the pBasex-algorithm.

the different photoelectron contributions as different *energy channels* at nominal kinetic energies of 0.8 eV, 1.0 eV and 1.2 eV, and infer their origin, i.e. the excitation pathway, from the *angular* distribution. Both multi-photon excitation pathways proceed via the intermediate, non-resonant state $3p$, which is only transiently populated. However, since ionization takes place *during* the excitation also photoelectrons from this state are detected at low kinetic energies around 0.2 eV (blue arrows in Fig. 1). For more details see caption of Fig. 1.

2.2. Setup

In this section the experimental setup comprising the laser system and the photoelectron imaging spectrometer is described. Intense 795 nm, 30 fs FWHM (Full Width at Half Maximum) laser pulses provided by an amplified 1 kHz Ti:sapphire laser system (*Femtolasers Femtopower Pro*) were phase modulated in frequency domain by a home-built pulse shaper [53], applying quadratic phase masks of the form $\varphi_{mod}(\omega) = \varphi_2/2 \cdot (\omega - \omega_0)^2$, where ω_0 is the central frequency of our laser spectrum [27]. The chirp parameter φ_2 was varied in the range from -2000 fs^2 to $+2000 \text{ fs}^2$ in steps of $\Delta\varphi_2 = 100 \text{ fs}^2$. The chirped output pulses of $12 \mu\text{J}$ energy were sent into a vacuum chamber and refocused by a concave mirror (5 cm focal length; we estimated a *peak* intensity of about 10^{13} W/cm^2 for the bandwidth-limited pulse) into sodium vapor supplied by an alkali metal dispenser source, as shown in Fig. 2. Photoelectrons released during the strong-field interaction of the shaped pulses with single atoms were detected by a photoelectron imaging spectrometer using the VMI method. In order to compensate the residual chirp of the unmodulated pulse, we performed an *in situ* adaptive optimization

of the multi-photon ionization of water vapor background (about 4×10^{-7} mbar) in the interaction region of the spectrometer. The resulting optimal compensation phase was additionally applied to the pulse shaper during the experiments, ensuring an error in the chirp parameter φ_2 of less than 150 fs². The energy calibration of the imaging spectrometer was performed using a 3+1 REMPI of xenon atoms excited by a Nd:YAG ns laser system at 355 nm, achieving a spectrometer resolution of 60 meV at 0.5 eV. Employing the energy calibrated photoelectron imaging spectrometer we studied angular and energy resolved photoelectron spectra as a function of the chirp parameter φ_2 .

3. Experimental results and discussion

Figure 3 (upper row) shows measured PADs from REMPI of sodium atoms with chirped fs laser pulses for three exemplary values of the chirp parameter φ_2 . The middle row displays the corresponding Abel-inverted (retrieved) PADs obtained by employing the pBasex-algorithm [50, 54]. When PADs arise from ionization with polarization shaped pulses [55], direct tomography methods have been developed for three-dimensional reconstruction of ultrashort free photoelectron wave packets [56]. Angular sections through the retrieved PADs at kinetic energies 0.8 eV, 1.0 eV and 1.2 eV, as plotted in the lower row, serve to identify the symmetry of the different energy channels observed in the PADs. The PAD measured for the unmodulated, i.e., bandwidth-limited pulse is depicted in the central column. Three major contributions are observed at kinetic energies 0.8 eV, 1.0 eV and 1.2 eV, related to the energy channels discussed above (cf. Sect. 2.1). The angular section taken at 1.2 eV exhibits two minor nodes between 0° and 180°, i.e. *d*-symmetry. This channel is attributed mainly to ionization via state *7p* (red excitation pathway in Fig. 1), though our numerical simulations (inset of Fig. 4) indicate, that also ionization via state *6f* (green excitation pathway in Fig. 1) delivers a minor contribution. The contribution of an *s*-wave to this channel, as expected from the excitation scheme Fig. 1, is reflected in the *weak* equatorial signal: At an angle of 90° *s* and *d*-wave have opposite sign and, thus, interfere destructively, whereas at the poles, i.e. at 0° and 180°, both waves add up constructively. The section taken at 1.0 eV exhibits 4 nodes between 0° and 180°, corresponding to *g*-symmetry. This contribution originates predominantly from ionization via state *5f*. The observation that the lobe at 90° (and 270° respectively) is slightly lowered with respect to its two neighbors indicates a weak *d*-wave contribution interfering destructively with the *g*-wave in this angular segment. The contribution measured at 0.8 eV shows again combined *s* and *d*-symmetry and is ascribed to ionization via state *5p*.

Moreover, a weak contribution is observed at about 0.2 eV, a magnification of which is shown in the inset of Fig. 3(b). The nodal structure of this signal exhibits distinct *f*-symmetry. However, the pronounced poles of the PAD as well as the fact, that the nodes at 45° and 135° in the angular section are raised with respect to the node at 90° give a hint on a *p*-wave contribution to the photoelectron signal. Observation of photoelectron wave packets with combined *p* and *f*-symmetry close to the ionization threshold is

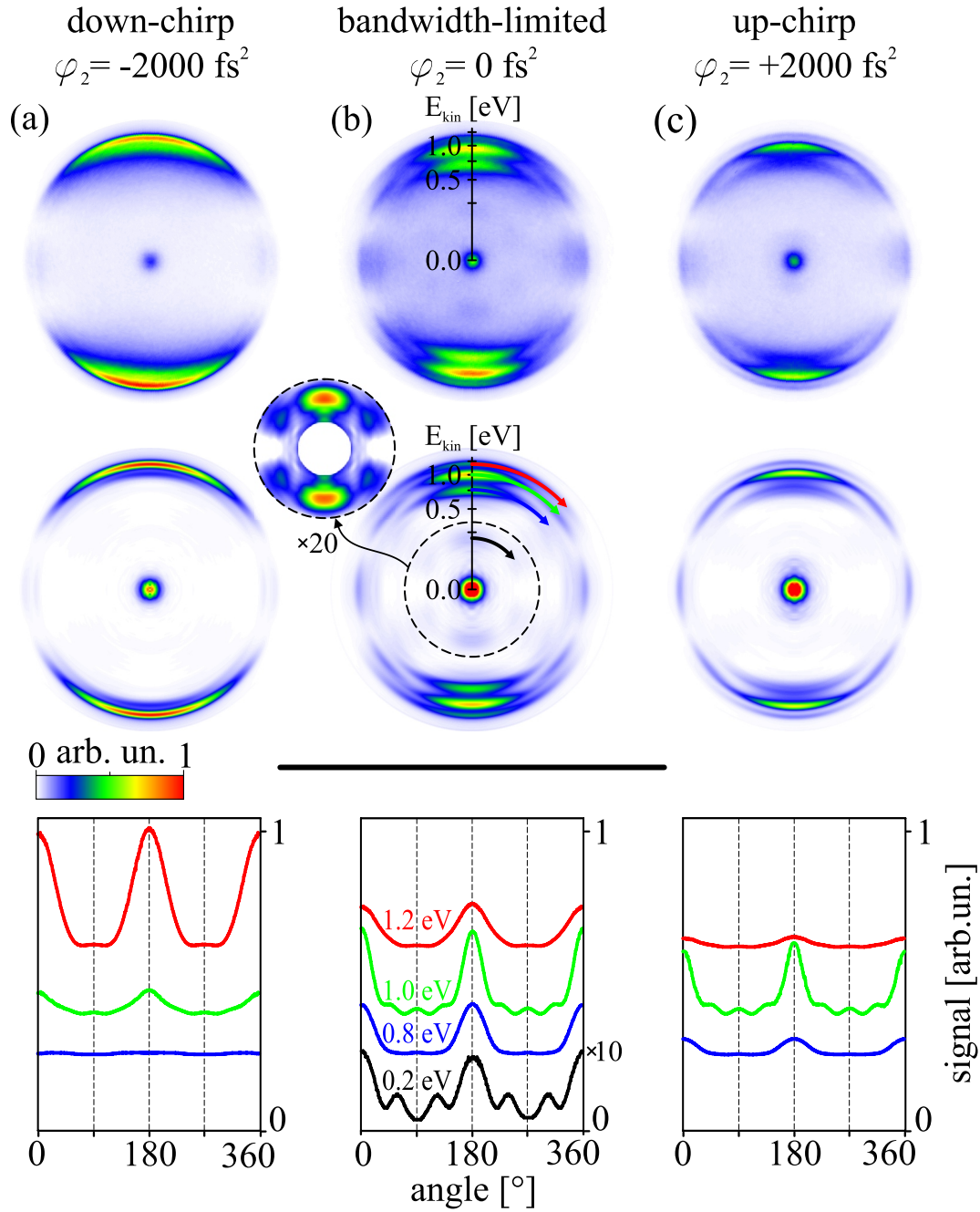


Figure 3. (Color online) measured PADs from excitation and ionization of sodium atoms using both chirped and bandwidth-limited fs laser pulses. In the upper row measured PADs for different values of the chirp parameter φ_2 are shown. (a) $\varphi_2 = -2000 \text{ fs}^2$ (down-chirp). (b) $\varphi_2 = 0$ (bandwidth-limited). (c) $\varphi_2 = +2000 \text{ fs}^2$ (up-chirp). All images are scaled to the same maximum value. The middle row contains the corresponding Abel-inverted PADs obtained using the pBasex-algorithm. Angular sections through the retrieved PADs at kinetic energies of about 0.2 eV, 0.8 eV, 1.0 eV and 1.2 eV (lower row) reveal the symmetries of the observed contributions and shed light on the underlying ionization pathways. The signal offsets are introduced for better visibility.

consistent with two-photon ionization from state $3p$ (blue pathway in Fig. 1). Note, that state $3p$ is—although non-resonant—transiently populated during the interaction, mediating the multi-photon processes to the state $4s$ and the high lying f states.

For large negative values of φ_2 (left column in Fig. 3), i.e. strongly *down*-chirped laser pulses, the outer channel at kinetic energy 1.2 eV is considerably enhanced in comparison to the bandwidth-limited case, whereas the intermediate channel at 1.0 eV is strongly reduced and the two innermost contributions have essentially vanished. Note the change in symmetry of the intermediate channel which exhibits combined s and d -symmetry in this case, indicating more efficient ionization from state $6p$, while the $5f$ contribution is very small. Changing the sign of φ_2 , i.e. using strongly *up*-chirped laser pulses (right column in Fig. 3), suppresses the high energy channel in favor of the intermediate channel at 1.0 eV which dominates the PAD in this case. From its angular section at 1.0 eV we find a combined d and g -symmetry, as in the bandwidth-limited case. This contribution is therefore traced back mainly to state $5f$. The finding that the symmetry of photoelectrons from the intermediate channel alters from d to g is rationalized by the change of the ordering of red and blue frequency components within the chirped pulse. For a down-chirped pulse, i.e. when the blue components arrive first, initially, the system is in resonance with the two-photon transition $4s \leftarrow \leftarrow 3s$ implying efficient ionization via the p states (red pathway in Fig. 1). On the other hand, up-chirped pulses favor ionization via state $5f$ since at early times the system is in resonance with the three-photon transition $5f \leftarrow \leftarrow \leftarrow 3s$ (green pathway in Fig. 1). Such processes have also been observed in [39] under different excitation conditions.

In order to provide the full picture of the chirp dependent population flow to the different energy channels, we performed an angular integration of all 41 measured PADs and present the resulting energy-resolved photoelectron spectra in terms of a two-dimensional map as a function of the kinetic energy and the chirp parameter φ_2 . The result obtained upon variation of φ_2 in the range from -2000 fs^2 to $+2000 \text{ fs}^2$ is displayed in Fig. 4. The three major channels at 0.8 eV, 1.0 eV and 1.2 eV are clearly visible. Note, that for e.g. rare gas atoms under our experimental conditions ponderomotive shifts of more than 0.5 eV are calculated. No such shifts are observed in the experiment, since the high-frequency approximation [57, 58] (necessary condition for the application of the ponderomotive energy concept) is not valid for alkalis excited by near infrared laser radiation. An analysis of the neutral excitation dynamics behind the observed contributions will be given in Sec. 4. The map illustrates the above statements, that for large negative values of φ_2 the high energy channel at 1.2 eV is addressed with high efficiency, i.e. a down-chirped pulse steers the population predominantly towards the high lying state $7p$. For large positive chirp values the intermediate channel is selectively addressed, corresponding to predominant population of states $6p$ and $5f$. The low energy channel is accessed most efficiently in the vicinity of $\varphi_2 = 500 \text{ fs}^2$. In fact, in the regime $0 \leq \varphi_2 \leq 1000 \text{ fs}^2$ the photoelectron spectrum is made up of contributions from states $5p$, $6p$ and $5f$. Because the excitation (and simultaneous ionization) takes place on an ultrashort time scale precluding decoherence processes, a *coherent* superposition of

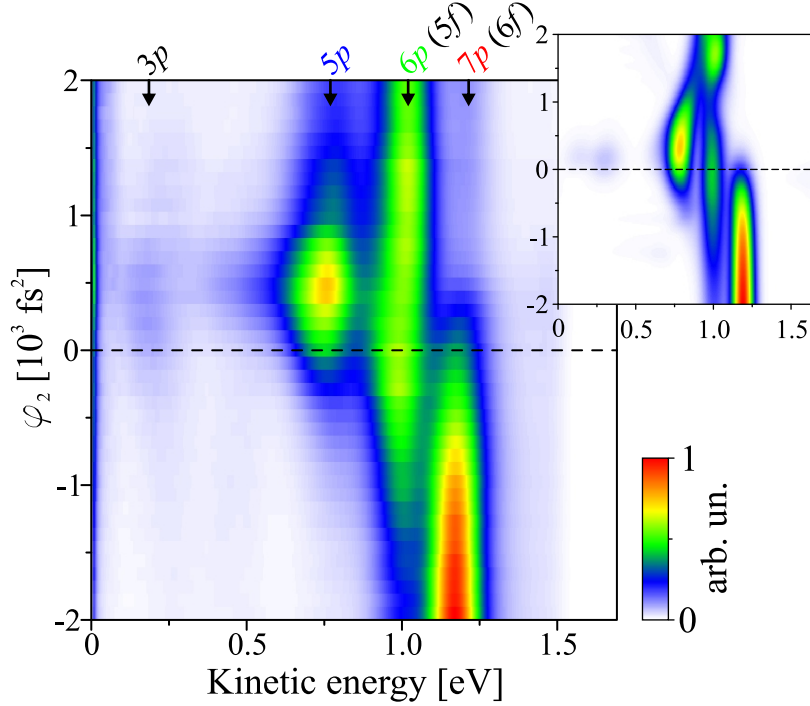


Figure 4. (Color online) measured photoelectron kinetic energy distributions as a function of the chirp parameter φ_2 . The data were obtained by angular integration of the retrieved PADs. Three main energy channels are observed at 0.8 eV, 1.0 eV and 1.2 eV, each of which can be activated by appropriate choice of the chirp parameter. For $\varphi_2 \ll 0$, i.e. strongly down-chirped laser pulses, photoelectrons with high kinetic energies related to the high lying states $7p$ (and minor $6f$ contribution) are produced. The intermediate channel at 1.0 eV, related to states $6p$ and $5f$, is addressed by strongly up-chirped laser pulses with $\varphi_2 \gg 0$. Photoelectrons with kinetic energies around 0.8 eV, corresponding to state $5p$, are favored at small positive values of φ_2 , i.e. high laser pulse peak intensities. The weak contribution at 0.2 eV in the same φ_2 -region stems from ionization of the non-resonant state $3p$. The inset shows results from a numerical simulation of the multi-photon excitation and ionization process.

states $5p$, $6p$ and $5f$ is excited in this chirp regime. Upon changing the sign of φ_2 , i.e. for $-1000 \text{ fs}^2 \leq \varphi_2 \leq 0$, the laser pulse induces a coherent superposition of states $6p$, $5f$ and $7p$. Photoelectrons observed at about 0.2 eV for moderate positive chirps are attributed to two-photon ionization from state $3p$.

The inset to Fig. 4 shows results from a numerical simulation of the simultaneous multi-photon excitation and ionization process. The calculations are based on numerical integration of the time-dependent Schrödinger-equation for a neutral 20-state system (comprising those states labeled in Fig. 1 and taking the fine structure splitting into account) interacting with an intense chirped 795 nm, 30 fs FWHM Gaussian input pulse. One-photon ionization from the high lying p and f states is treated within a simplified model employing first order perturbation theory. We assume a flat continuum and unit coupling elements with no additional phases for all bound-free transitions. A more rigorous treatment of the ionization step involving the determination of radial coupling

matrix elements also for the bound-free transitions is provided by, e.g., single-channel quantum defect theory [59] as reported for instance in [60, 61]. In order to model the two-photon ionization from state $3p$ proceeding, for example, via state $3d$ as indicated by the blue pathway in Fig. 1, we employed second order perturbation theory. For a more detailed description of our method see [25, 27, 62]. The simulation of photoelectron spectra reproduces the main features of the experimental results very well. This allows us to look into the underlying *neutral* excitation dynamics and follow the population flow within the bound atomic system. We find that for *large negative chirp* φ_2 state $7p$ is addressed almost selectively, while for large positive φ_2 values both states $6p$ and $5f$ are populated efficiently in equal measure. The latter is in accordance with the experimental observation of the PAD with pronounced *g*-symmetry in the intermediate channel at 1.0 eV for *large positive chirp* (see Fig. 3(c)). The most efficient excitation of state $5p$ occurs for *moderate positive chirp*. However, in this chirp regime states $6p$ and $5f$ receive comparable population confirming the observation of a PAD with a contribution of *g*-symmetry at 1.0 eV and *zero chirp*. At *moderate negative chirp*, we obtain a coherent superposition of states $6p$, $5f$ and $7p$. Note that the weak contribution around 0.2 eV and small positive values of φ_2 observed in the experiment (shown in the inset to Fig. 3(b)) is also reproduced in the simulation. Within the framework of our simulation, these photoelectrons are ascribed to two-photon ionization from state $3p$ which receives non-perturbative *transient* population. We note, that in a perturbative regime, ionization from this transiently populated state could be interpreted as a transition from a *virtual* state.

In the next section, we will further investigate the neutral population dynamics by means of a reduced atomic system in order to rationalize the general features observed in the experiment in terms of physical mechanisms governing the excitation process.

4. Theoretical model

In this section we provide a mainly qualitative description of the system at hand. To this end, we assume that the photoelectron signal arises most significantly through the 2+1+1 REMPI channel (red pathway in Fig. 1), involving the five states $3s$, $4s$, $5p$, $6p$ and $7p$. The idea of this reduction is to demonstrate the basic principles influencing the dynamics of the whole system, which become more transparent in this simplified model, involving the most significant states for our experiment. In this approach, we adiabatically eliminated state $3p$ [44, 63, 64] because it is off resonance and receives smaller transient population than the other coupled states. Its presence, though, affects the population dynamics significantly for it induces strong dynamic Stark-shifts in the energies of states $3s$ and $4s$, which substantially modify the energy diagram.

The quantum dynamics of this five-state system obeys the time-dependent Schrödinger equation

$$i\hbar \frac{d}{dt} \mathbf{c}(t) = \mathbf{H}(t) \mathbf{c}(t). \quad (1)$$

The Hamiltonian $\mathbf{H}(t)$ in the rotating-wave approximation, rotating with the instantaneous laser frequency $\omega(t) = \omega_0 + 2at$ (see Eq. (A.5) in the appendix), is given by [44, 64]:

$$\mathbf{H}(t) = \hbar \begin{bmatrix} \Delta_1 - S_1 & \frac{1}{2}\Omega_{12} & 0 & 0 & 0 \\ \frac{1}{2}\Omega_{12} & \Delta_2 - S_2 & \frac{1}{2}\Omega_{23} & \frac{1}{2}\Omega_{24} & \frac{1}{2}\Omega_{25} \\ 0 & \frac{1}{2}\Omega_{23} & \Delta_3 & 0 & 0 \\ 0 & \frac{1}{2}\Omega_{24} & 0 & \Delta_4 & 0 \\ 0 & \frac{1}{2}\Omega_{25} & 0 & 0 & \Delta_5 \end{bmatrix}. \quad (2)$$

Here the explicit time dependence is dropped for ease of notation. The vector $\mathbf{c}(t) = [c_1(t), c_2(t), \dots, c_5(t)]^T$ consists of the amplitudes of the five states, ordered as shown above, which are obtained by numerical integration of the Schrödinger-equation (1), the respective populations are $P_n(t) = |c_n(t)|^2$, $\Delta_n(t) = \omega_n - k\omega(t)$ are the generally time-dependent atom-laser detunings, where ω_n are the atomic state eigenfrequencies, with ω_{3s} taken as zero, k is the transition order, $\Omega_{2n} = d_{2n}\Omega_0 f(t)$ represent the one-photon couplings of state 2 to state n ($n = 3, 4, 5$), $\Omega_{12} = q_{12}\Omega_0^2 f^2(t)$ is the two-photon coupling between states 1 and 2, with $f(t)$ being the chirped laser electric field envelope, d_{mn} are the relevant transition dipole moments in atomic units, q_{12} is the effective two-photon transition moment (cf. Eq. (A.1)) and S_1 and S_2 represent the DSS of states 1 and 2, respectively,

$$S_1 = \frac{\Omega_{3s3p}^2}{4\Delta_{3p}}, \quad S_2 = \frac{\Omega_{3p4s}^2}{4\Delta_{3p}}. \quad (3)$$

The effect of the DSS due to state $3d$ is neglected for it is very weakly coupled to the states whose energies it might influence: the p states are coupled about 10 times stronger to state $4s$ as compared to state $3d$; state $3d$ is not directly coupled to state $3s$, but rather through a two-photon transition. In the first two diagonal elements of the Hamiltonian (associated with the energies of states $3s$ and $4s$) the atom-laser detuning and the DSS add up to a time-dependent *effective* chirp: the former resulting from the time-dependent instantaneous laser frequency $\omega(t)$, and the latter deriving from the time-dependent shift of the level energies due to DSS.

4.1. Excitation regimes

In Fig. 5 we distinguish five different regimes in regard to the value of the chirp φ_2 . In all cases we plot the bare-state energies and analyze the dynamics by accounting for the presence of level crossings. Because it is the ionization signal that is observed in the experiment it is also important *when* a particular level crossing occurs: a level crossing at *early* time, and the ensuing adiabatic passage transition, would translate into a larger ionization signal than a *late* crossing, where even a significant population transfer to a certain discrete state would not be reflected in the ionization signal.

Below we examine the dynamics of our system with particular interest in states $5p$, $6p$ and $7p$. In Fig. 5 we show the populations and the energies of the five bare states for

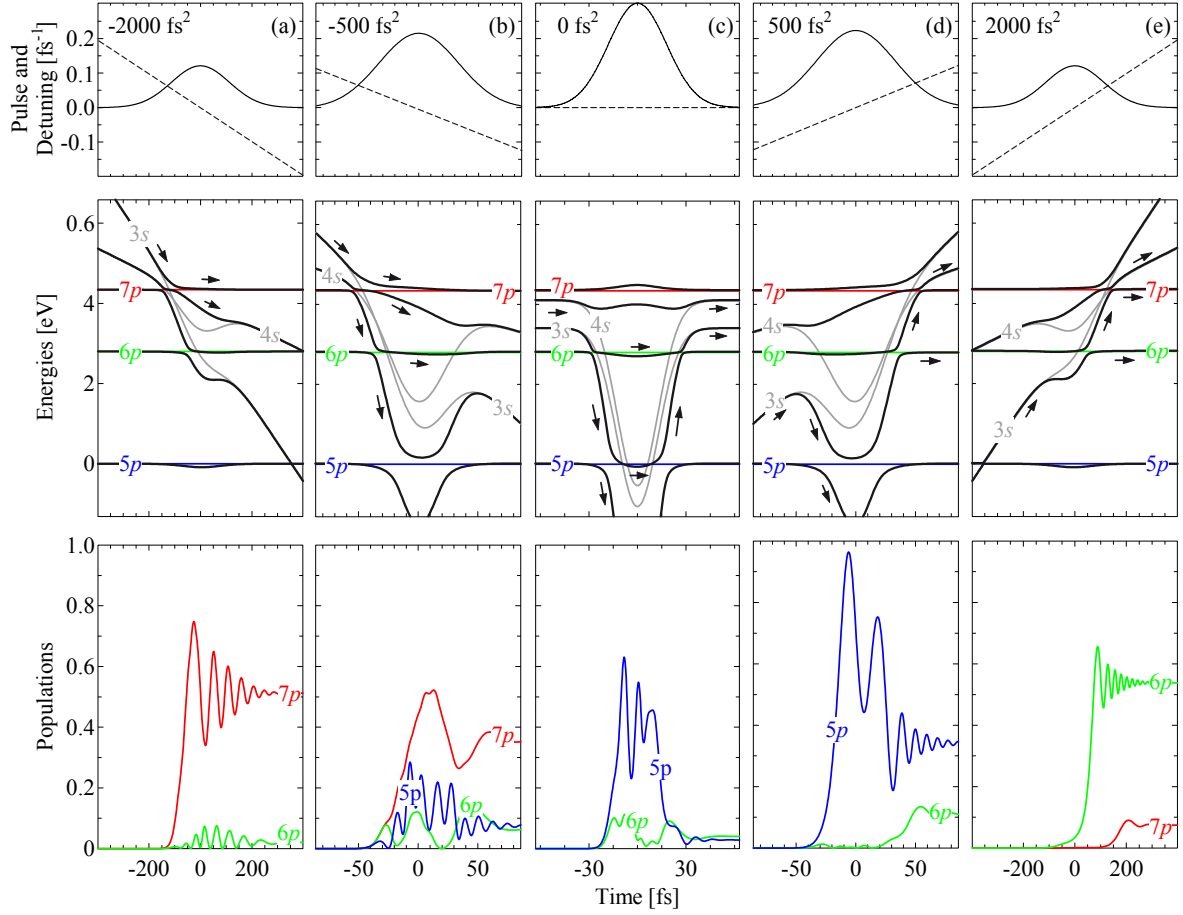


Figure 5. (Color online) populations (lower frames) and energies (middle frames) of the states of interest $5p$, $6p$ and $7p$ vs time for φ_2 varied (from left to right) between -2000 fs^2 (down-chirp) and 2000 fs^2 (up-chirp), $\Omega_0 = 0.3 \text{ fs}^{-1}$ and $\Delta t = 30 \text{ fs}$. In the middle frames, colored and grey lines depict the bare state energies. The latter are related to states $3s$ and $4s$ and include the effective chirp, i.e. the chirp of the laser as well as the chirp due to ac Stark-shifts. Black lines represent the dressed state energies and the arrows are to show the population flow. The populations in the lower frames are consistent with the asymmetry in the experimental results presented in Fig. 4: for large chirps states $6p$ (positive chirp) and $7p$ (negative chirp) are predominantly populated, whereas around zero chirp the contribution comes mostly from state $5p$. The envelopes (straight lines) and detunings (dashed lines) of the modulated pulses are shown in the uppermost frames. Note that the energies are mirrored when changing the sign of the chirp φ_2 .

the chirp φ_2 varied between -2000 fs^2 and 2000 fs^2 (from left to right) with the system initiated in state $3s$. For illustrative purposes we pick $\Omega_0 = 0.3 \text{ fs}^{-1}$, corresponding to an intensity of $3.7 \times 10^{12} \text{ W/cm}^2$ [63], and $\Delta t = 30 \text{ fs}$.

4.1.1. Large negative chirp For large negative chirp ($\varphi_2 = -2000 \text{ fs}^2$, Fig. 5(a)) the laser field reaches resonances relative to the $7p \leftarrow 4s$ (one-photon) transition and the $4s \leftarrow 3s$ (two-photon) transition in nearly the same instant, thus creating a “bow-tie” level crossing pattern [44, 65, 66, 67, 68, 69] which is of particular significance because

it involves three rather than two states. This crossing results in efficient population transfer to states $4s$ and $7p$ and depopulation of state $3s$. Because state $7p$ is populated at such early times, it is exposed to ionization for most of the interaction dynamics and hence has a dominant contribution in the photoelectron signal (see Fig. 4 at 1.2 eV and -2000 fs^2).

Later on we observe almost adiabatic evolution and the population is shared mainly between states $4s$ and $7p$ in the form of Rabi-oscillations with fading amplitude [70]. State $6p$ acquires only marginal population mainly due to its crossing with state $3s$ (which is, however, already depleted due to the preceding “bow-tie” crossing) via a three-photon excitation through state $4s$. The late crossings between states $3s$ and $5p$, and also between states $4s$ and $6p$ are of no importance because they occur after the pulse intensity has essentially vanished. State $5p$ remains unpopulated since it is far off-resonant throughout the entire dynamics.

4.1.2. Large positive chirp For large positive chirps ($\varphi_2 = 2000 \text{ fs}^2$, Fig. 5(e)) the energy diagram is mirrored compared to the one for large negative chirps φ_2 (Fig. 5(a)). Then initially the system evolves adiabatically, with minor (off-resonant) population transfer from state $3s$ to state $4s$ due to their strong mutual coupling. Around the time of the peak laser intensity, as state $3s$ sweeps across resonance with $6p$, the latter starts to effectively populate through the three-photon $3s - 6p$ crossing. Because this crossing occurs approximately in the middle of the laser pulse the population of state $6p$ is exposed to ionization for a considerable time interval, which results in significant photoelectron signal from $6p$ (see Fig. 4 at 1.0 eV and $+2000 \text{ fs}^2$). For the same reason—the $3s - 6p$ crossing occurring near the laser pulse maximum—the population transfer from state $3s$ to state $6p$ is relatively efficient and only about half of the population is left in states $3s$ and $4s$ thereafter; then only a part of this already reduced population is transferred to state $7p$ at the subsequent “bow-tie” crossing $3s - 4s - 7p$. Moreover, this crossing occurs at late times and hence state $7p$ is not visible in the photoelectron spectrum. State $5p$ remains unpopulated once again as it stays far off any resonance.

We now turn our attention to the regimes of a moderately large chirp φ_2 , where the photoelectron spectrum changes from a single-state feature to one displaying double features.

4.1.3. Moderate negative chirp For a moderate negative chirp ($\varphi_2 = -500 \text{ fs}^2$, Fig. 5(b)) an early crossing occurs between states $3s$, $4s$ and $7p$ in the rising edge of the pulse, which leads to a partial population transfer from state $3s$ to states $4s$ and $7p$, because the laser intensity is not strong enough to enforce adiabatic evolution. The population in state $7p$ is exposed to ionization for the rest of the pulse, whereas the population in state $4s$ proceeds until the subsequent $4s - 6p$ crossing where it is partially transferred to state $6p$. The leftover temporary flows into state $5p$, which starts to emerge in the photoelectron spectrum, and is finally driven back into state $3s$. In result, all states $5p$, $6p$ and $7p$ are visible in the photoelectron signal, which is

an indication for the creation of a coherent superposition of these (see Fig. 4 at about -500 fs^2).

4.1.4. Moderate positive chirp For moderate positive chirps ($\varphi_2 = 500 \text{ fs}^2$, Fig. 5(d)) state $3s$ first comes very close to state $5p$ at times of the laser pulse maximum; during this proximity the population undergoes Rabi-type oscillations between states $3s$ and $5p$ and is exposed to ionization from state $5p$. The signature of state $5p$ is clearly visible and indeed, this is the regime where this state indisputably dominates in the photoelectron signal (see Fig. 4 at 0.8 eV and $+500 \text{ fs}^2$). In other words, it is the DSS induced by the two-photon transition $4s \leftarrow\leftarrow 3s$, which makes the population of the far-off-resonant state $5p$ possible [71]. If this Stark-shift were absent (e.g. if the two-photon transition $4s \leftarrow\leftarrow 3s$ were instead a single-photon one in a gedanken scenario) state $5p$ would never receive sizeable population. As we proceed beyond the pulse maximum state $3s$ crosses state $6p$ and the population is partially transferred to the latter. Hence state $6p$ emerges in the photoelectron signal due to the ensuing ionization, whereas state $7p$ is invisible in this regime because all population left flows into state $4s$.

4.1.5. Zero chirp. In this regime the laser pulse is unchirped, $\varphi_2 = 0$. Therefore, the *effective* chirp is entirely due to ac Stark-shift. The latter is symmetric to the pulse because it is induced by the same pulse. Moreover, because state $3s$ crosses states $6p$ and $5p$ (Fig. 5(c)), sizeable population will visit these two states through the respective first crossings $3s - 5p$ and $3s - 6p$. A second pair of crossings in the falling edge of the pulse will induce additional transitions $5p \leftarrow\leftarrow\leftarrow 3s$ and $6p \leftarrow\leftarrow\leftarrow 3s$. The implication is that states $5p$ and $6p$ will contribute significantly to the photoelectron signal (see Fig. 4 around $\varphi_2 = 0$). State $7p$, on the other hand, remains well off resonance throughout and receives only a small population due to (weak) non-resonant interaction. Its contribution to the photoelectron signal should be therefore more muted than these from states $5p$ and $6p$.

4.2. Discussion

Below we discuss the five excitation regimes in the dressed state (adiabatic) context. When adiabatic, which demands large couplings and low chirp rates for the avoided crossings in question, starting in state $3s$ we end up in state $7p$ for $\varphi_2 < 0$ or in state $6p$ for $\varphi_2 > 0$ (Fig. 5, middle frames; in the latter case a fully non-adiabatic passage across state $5p$ occurs, since the pulse intensity is negligible for the $3s - 5p$ resonance). Therefore, clearly from Fig. 5, our system exhibits a somewhat adiabatic behavior for chirp φ_2 away from the origin. As we get closer, the crossings shift towards the pulse wings, whereas the pulse gets narrower in time, which in combination results in breaking adiabaticity. The latter is further hindered by the increased DSS, which effectively enhances the chirp rate.

We expect adiabaticity to remain almost unaffected for large negative values of

the chirp φ_2 , since the chirp rate $a \propto 1/\varphi_2$ and $\Omega \propto 1/\sqrt{\varphi_2}$, and to break down for large positive values, for it relies on the three-photon transition $6p \leftarrow \leftarrow \leftarrow 3s$, which gets weaker, as the resonances relative to $3s - 4s$ and $4s - 6p$ further separate in time. Larger peak intensities Ω_0 strengthen adiabaticity for the transition $7p \leftarrow \leftarrow \leftarrow 3s$ and make complete population transfer possible, as also indicated in [34], whereas for the transition $6p \leftarrow \leftarrow \leftarrow 3s$ due to the unfavorable influence of the increased DSS we predict the contrary.

5. Summary and Conclusion

In this contribution we presented a joint experimental and theoretical study on strong-field Resonance Enhanced Multi-Photon Ionization (REMPI) of sodium atoms using chirped femtosecond laser pulses. Experimentally, Photoelectron Angular Distributions (PADs) have proven the essential tool to identify the different excitation and ionization pathways.

We observed three distinct ionization pathways contributing to the measured PADs. The predominant contribution with combined s and d -symmetry is due to a 2+1+1 REMPI processes involving the strongly driven two-photon transition $4s \leftarrow \leftarrow 3s$, and subsequent ionization from the states $5p$, $6p$ and $7p$. Photoelectrons with combined d and g -symmetry originated from 3+1 REMPI via states $5f$ and $6f$. A weak contribution with combined p and f -symmetry close to the ionization threshold is attributed to the third channel, that is two-photon ionization of the non-resonant transiently populated state $3p$.

Selective population of the highly excited states $5p$, $6p$, $7p$ and $5f$, $6f$ was achieved by controlling a single pulse parameter, i.e. the chirp parameter φ_2 . In particular, we observed highly selective population of state $7p$ using strongly down-chirped laser pulses. For strongly up-chirped laser pulses states $6p$ and $5f$ were populated with high efficiency and a dominant signal from state $5p$ was obtained for moderately up-chirped laser pulses. Moreover, in the intermediate chirp regions coherent superpositions of neighboring states have been excited.

Simulations based on numerical integration of the time-dependent Schrödinger-equation for a neutral 20-state system are in agreement with our experimental findings. In addition, a five-state model was developed in order to provide insights into the physical mechanisms at play. Our analysis of the time-dependent populations showed that by tuning the chirp parameter distinct physical mechanisms have been addressed, involving adiabatic and non-adiabatic time evolution along with Dynamic Stark-Shifts (DSSs) and (multiple) level crossings. It was pointed out that the occurrence of an uncommon “bow-tie” level crossing is responsible for the excitation of coherent superposition states as observed in the experiment. The strong DSS of the two-photon transition $4s \leftarrow \leftarrow 3s$ turned out to be of particular significance for populating state $5p$ being inaccessible in weak laser fields.

Our results highlight the importance of studying model systems experimentally

and theoretically to better understand the physical mechanisms of strong-field coherent control. Our findings demonstrate that, in general, in strong-field control multiple pathways involving different physical mechanisms are at play simultaneously.

Appendix A. Details of calculations

Each p state consists of $p_{1/2}$ and $p_{3/2}$ substates, coupled by $\Omega_{1/2}$ and $\Omega_{3/2}$, respectively, to a relevant s state. Therefore initially our system comprises overall 10 states (prior to eliminating state $3p$). To simplify our approach we perform a transformation to a dark-bright basis for each of the p states and thus eliminate half of the p substates as dark (uncoupled) states, and keep the rest, which become coupled by the root mean square of the relevant $\Omega_{1/2}$ and $\Omega_{3/2}$ and are the ones to be referred to as p states throughout the theoretical part of the paper.

The effective two-photon transition moment between states $3s$ and $4s$ is

$$q_{12} = -\frac{d_a d_b + d_c d_d}{2\Delta_{3p}}, \quad (\text{A.1})$$

where $d_{a,c}$ and $d_{b,d}$ are the dipole moments for the transitions $3p_{1/2,3/2} \leftarrow 3s_{1/2}$ and $4s_{1/2} \leftarrow 3p_{1/2,3/2}$, respectively.

The effect of a quadratic phase modulation in frequency domain of the form

$$\varphi(\omega) = \frac{\varphi_2}{2}(\omega - \omega_0)^2 \quad (\text{A.2})$$

is described in time domain by a modulated linearly polarized laser electric field $E(t)$ given as [72]

$$E(t) = 2\text{Re}\{E^+(t)\}, \quad (\text{A.3})$$

where for the positive-frequency part we have

$$E^+(t) = \frac{E_0}{2\gamma^{1/4}} e^{-\frac{t^2}{4\beta\gamma}} e^{i\omega_0 t} e^{i(at^2 - \varepsilon)} \quad (\text{A.4})$$

with

$$\begin{aligned} \varepsilon &= \frac{1}{2} \arctan \frac{\varphi_2}{2\beta}, \\ \beta &= \frac{\Delta t^2}{8 \ln 2}, \\ \gamma &= 1 + \left(\frac{\varphi_2}{2\beta} \right)^2, \\ a &= \frac{\varphi_2}{8\beta^2\gamma} \end{aligned}$$

resulting in the time-dependent instantaneous laser frequency

$$\omega(t) = \omega_0 + 2at. \quad (\text{A.5})$$

Here Δt denotes the FWHM of the intensity $I(t)$ of the unmodulated pulse, ω_0 is the laser carrier frequency and φ_2 is the chirp parameter to be varied.

We define a reference Rabi-frequency $\Omega(t) = \Omega_0 f(t)$, where $f(t)$ is the laser electric field envelope

$$f(t) = \frac{\exp\left(-\frac{t^2}{4\beta\gamma}\right)}{\gamma^{1/4}}. \quad (\text{A.6})$$

Acknowledgments

Discussions with P. Lambropoulos and F. Faisal regarding the measured photoelectron signals assigned to two-photon ionization from state $3p$ are gratefully acknowledged. The Kassel group furthermore acknowledges financial support by the Deutsche Forschungsgemeinschaft DFG. This work has also been supported by European Commission projects EMALI and FASTQUAST, and the Bulgarian NSF grants VU-F-205/06, VU-I-301/07, D002-90/08, and IRC-CoSiM.

References

- [1] T. Baumert, J. Helbing, G. Gerber, in *Advances in Chemical Physics* (Wiley, 1997)
- [2] S. Rice, M. Zhao, *Optical Control of Molecular Dynamics* (Wiley, 2000)
- [3] M. Shapiro, P. Brumer, *Principles of the Quantum Control of Molecular Processes* (Wiley, 2003)
- [4] H. Rabitz, R. de Vivie-Riedle, M. Motzkus, K. Kompa, *Science* **288**, 824 (2000)
- [5] R. Levis, H. Rabitz, *J. Phys. Chem. A* **106**, 6427 (2002)
- [6] M. Dantus, V. Lozovoy, *Chem. Rev.* **104**, 1813 (2004)
- [7] M. Wollenhaupt, V. Engel, T. Baumert, *Annu. Rev. Phys. Chem.* **56**, 25 (2005)
- [8] T. Brixner, T. Pfeifer, G. Gerber, M. Wollenhaupt, T. Baumert, in *Femtosecond Laser Spectroscopy* (Springer, 2005)
- [9] D. Tannor, *Introduction to Quantum Mechanics* (University Science Books, 2006)
- [10] H. Fielding, T. Baumert, M. Shapiro (eds), *J. Phys. B* **41**, *Special Issue on Coherent Control* (2008)
- [11] R. S. Judson, H. Rabitz, *Phys. Rev. Lett.* **68**, 1500 (1992)
- [12] A. Assion, T. Baumert, M. Bergt, T. Brixner, B. Kiefer, V. Seyfried, M. Strehle, G. Gerber, *Science* **282**, 919 (1998)
- [13] T. Baumert, T. Brixner, V. Seyfried, M. Strehle, G. Gerber, *Appl. Phys. B* **65**, 779 (1997)
- [14] D. Meshulach, D. Yelin, Y. Silberberg, *Opt. Comm.* **138**, 345 (1997)
- [15] C. J. Bardeen, V. V. Yakolev, K. R. Wilson, S. D. Carpenter, P. M. Weber, W. S. Warren, *Chem. Phys. Lett.* **280**, 151 (1997)
- [16] M. Wollenhaupt, A. Assion, O. Bazhan, C. Horn, D. Liese, C. Sarpe-Tudoran, M. Winter, T. Baumert, *Phys. Rev. A* **68**, 015401 (2003)
- [17] N. Dudovich, T. Polack, A. Pe'er, Y. Silberberg, *Phys. Rev. Lett.* **94**, 083002 (2005)
- [18] C. Trallero-Herrero, J. L. Cohen, T. Weinacht, *Phys. Rev. Lett.* **96**, 063603 (2006)
- [19] S. Zhdanovich, E. A. Shapiro, M. Shapiro, J. W. Hepburn, V. Milner, *Phys. Rev. Lett.* **100**, 103004 (2008)
- [20] T. Bayer, M. Wollenhaupt, C. Sarpe-Tudoran, T. Baumert, *Phys. Rev. Lett.* **102**, 023004 (2009)
- [21] T. Frohnmeier, M. Hofmann, M. Strehle, T. Baumert, *Chem. Phys. Lett.* **312**, 447 (1999)
- [22] B. J. Sussman, D. Townsend, M. Y. Ivanov, A. Stolow, *Science* **314**, 278 (2006)
- [23] J. González-Vázquez, I. R. Sola, J. Santamaria, V. S. Malinovsky, *Chem. Phys. Lett.* **431**, 231 (2006)
- [24] M. Wollenhaupt, D. Liese, A. Präkelt, C. Sarpe-Tudoran, T. Baumert, *Chem. Phys. Lett.* **419**, 184 (2006)

- [25] M. Wollenhaupt, A. Präkelt, C. Sarpe-Tudoran, D. Liese, T. Bayer, T. Baumert, *Phys. Rev. A* **73**, 063409 (2006)
- [26] M. Wollenhaupt, T. Baumert, *J. Photochem. Photobiol. A* **180**, 248 (2006)
- [27] M. Wollenhaupt, A. Präkelt, C. Sarpe-Tudoran, D. Liese, T. Baumert, *Appl. Phys. B* **82**, 183 (2006)
- [28] T. Bayer, M. Wollenhaupt, T. Baumert, *J. Phys. B* **41**, 074007 (2008)
- [29] J. S. Melinger, S. R. Suketu, R. Gandhi, A. Hariharan, J. X. Tull, W. S. Warren, *Phys. Rev. Lett.* **68**, 2000 (1992)
- [30] P. Balling, D. J. Maas, L. D. Noordam, *Phys. Rev. A* **50**, 4276 (1994)
- [31] B. Chatel, J. Degert, S. Stock, B. Girard, *Phys. Rev. A* **68**, 041402 (2003)
- [32] G. P. Djotyan, J. S. Bakos, G. Demeter, P. N. Ignácz, M. Á. Kedves, Zs. Sörlei, J. Szigeti, Z. L. Tóth, *Phys. Rev. A* **68**, 053409 (2003)
- [33] T. Nakajima, *Phys. Rev. A* **75**, 053409 (2007)
- [34] S. D. Clow, C. Trallero-Herrero, T. Bergeman, T. Weinacht, *Phys. Rev. Lett.* **100**, 233603 (2008)
- [35] S. Ruhman, R. Kosloff, *J. Opt. Soc. Am. B* **7**, 1748 (1990)
- [36] S. Chelkowski, A. D. Bandrauk, P. B. Corkum, *Phys. Rev. Lett.* **65**, 2355 (1990)
- [37] J. S. Melinger, A. Hariharan, S. R. Suketu, R. Gandhi, W. S. Warren, *J. Chem. Phys.* **95**, 2210 (1991)
- [38] C. J. Bardeen, Q. Wang, C. V. Shank, *Phys. Rev. Lett.* **75**, 3410 (1995)
- [39] A. Assion, T. Baumert, J. Helbing, V. Seyfried, G. Gerber, *Chem. Phys. Lett.* **259**, 488 (1996)
- [40] V. V. Lozovoy, S. A. Antipin, F. E. Gostev, A. A. Tovbin, O. M. Sarkisov, A. S. Vetchinkin, S. Ya. Umanskii, *Chem. Phys. Lett.* **284**, 221 (1998)
- [41] N. T. Hashimoto, K. Misawa, R. Lang, *Appl. Phys. Lett.* **82**, 2749 (2003)
- [42] P. Nürnberger, G. Vogt, T. Brixner, G. Gerber, *Chem. Phys. Phys. Chem.* **9**, 2470 (2007) *and references therein*
- [43] A. Monmayrant, B. Chatel, B. Girard, *Phys. Rev. Lett.* **96**, 103002 (2006)
- [44] N. V. Vitanov, T. Halfmann, B. W. Shore, K. Bergmann, *Annu. Rev. Phys. Chem.* **52**, 763 (2001)
- [45] D. W. Chandler, P. L. Houston, *J. Chem. Phys.* **87**, 1445 (1987)
- [46] C. Bordas, F. Paulig, H. Helm, D. L. Huestis, *Rev. Sci. Instrum.* **67**, 2257 (1996)
- [47] A. T. J. B. Eppink, D. H. Parker, *Rev. Sci. Instrum.* **68**, 3477 (1997)
- [48] J. Winterhalter, D. Maier, J. Honerkamp, V. Schyja, H. Helm, *J. Chem. Phys.* **110**, 11187 (1999)
- [49] M. J. J. Vrakking, *Rev. Sci. Instrum.* **72**, 4084 (2001)
- [50] B. Whitaker, *Imaging in Molecular Dynamics* (Cambridge University Press, 2003)
- [51] National Institute of Standards and Technology, <http://www.nist.gov>
- [52] A. Präkelt, M. Wollenhaupt, C. Sarpe-Tudoran, T. Baumert, *Phys. Rev. A* **70**, 0634707 (2004)
- [53] A. Präkelt, M. Wollenhaupt, A. Assion, C. Horn, C. Sarpe-Tudoran, M. Winter, T. Baumert, *Rev. Sci. Instrum.* **74**, 4950 (2003)
- [54] G. A. Garcia, L. Nahon, I. Powis, *Rev. Sci. Instrum.* **75**, 4989 (2004)
- [55] M. Wollenhaupt, M. Krug, J. Köhler, T. Bayer, C. Sarpe-Tudoran, T. Baumert, *Appl. Phys. B* **95**, 245 (2009)
- [56] M. Wollenhaupt, M. Krug, J. Köhler, T. Bayer, C. Sarpe-Tudoran, T. Baumert, *Appl. Phys. B* (2009), in print
- [57] P. Avan, C. Cohen-Tannoudji, J. Dupont-Roc, C. Fabre, *J. de Phys.* **37**, 993 (1976)
- [58] A. L'Huillier, L. A. Lompré, D. Normand, X. Tang, P. Lambropoulos, *J. Opt. Soc. Am. B* **6**, 1790 (1989)
- [59] M. J. Seaton, *Rep. Prog. Phys.* **46**, 167 (1983)
- [60] S. N. Dixit, P. Lambropoulos, *Phys. Rev. A* **27**, 861 (1983)
- [61] G. Leuchs, S. J. Smith, S. N. Dixis, P. Lambropoulos, *Phys. Rev. Lett.* **56**, 708 (1986)
- [62] M. Wollenhaupt, T. Bayer, M. Krug, C. Sarpe-Tudoran, T. Baumert, *J. Phys. Conf. Ser.* **88**, 012053 (2007)
- [63] B. W. Shore, *The Theory of Coherent Atomic Excitation, Vol. I* (Wiley, New York, 1990)
- [64] B. W. Shore, *Act. Phys. Slov.* **58**, 243 (2008)

- [65] C. E. Carroll, F. T. Hioe, J. Phys. A **19**, 1151 (1986)
- [66] C. E. Carroll, F. T. Hioe, J. Phys. A **19**, 2061 (1986)
- [67] V. N. Ostrovsky, H. Nakamura, J. Phys. A **30**, 6939 (1997)
- [68] D. A. Harmin, Phys. Rev. A **44**, 433 (1991)
- [69] S. Brundobler, V. Elser, J. Phys. A **26**, 1211 (1993)
- [70] S. Zamith, J. Degert, S. Stock, B. de Beauvoir, V. Blanchet, M. A. Bouchene, B. Girard, Phys. Rev. Lett. **87**, 033001 (2001)
- [71] T. Rickes, L. P. Yatsenko, S. Steuerwald, T. Halfmann, B. W. Shore, N. V. Vitanov, K. Bergmann, J. Chem. Phys. **113**, 534 (2000)
- [72] M. Wollenhaupt *et al.*, in *Springer Handbook of Lasers and Optics*, Ch. 12 (Springer, 2007)